Proceedings of ASME Turbo Expo 2011
GT2011
June 6-10, 2011, Vancouver, British Columbia, Canada

GT2011-46247

SCATTERING OF PLANE WAVES BY A CONSTRICTION

E. Alenius*, **M. Åbom**
The Marcus Wallenberg Laboratory for Sound and Vibration Research
Department of Aeronautical and Vehicle Engineering
KTH
SE-100 44, Stockholm
Sweden
Email: ealenius@kth.se

L. Fuchs
Department of Mechanics
KTH
SE-100 44, Stockholm
Sweden

ABSTRACT

Liner scattering of low frequency waves by an orifice plate has been studied using Large Eddy Simulation and an acoustic two-port model. The results have been compared to measurements with good agreement for waves coming from the downstream side. For waves coming from the upstream side the reflection is over-predicted, indicating that not enough of the acoustic energy is converted to vorticity at the upstream edge of the plate. Furthermore, the sensitivity to the amplitude of the acoustic waves has been studied, showing difficulties to simultaneously keep the amplitude low enough for linearity and high enough to suppress flow noise with the relatively short times series available in LES.

INTRODUCTION

Constrictions are common elements in turbomachinery duct systems. These constrictions generate noise and scatter acoustic waves generated by other components. By reflecting and damping incoming waves the constrictions modify the resonances in the system, which may result in high sound levels and under certain conditions the performance of the machine can be affected. The noise generated by a constriction can normally be neglected compared to other sound sources in the system and hence will not be considered here. However, under certain flow configurations the constriction can cause a high tonal noise (whistle) if it couples to a resonance in the system, see e.g. [1]. The constriction studied in this work is a thin orifice plate, i.e. a plate with a centrally located sharp edged orifice, placed in a circular duct.

When a wave impinges on an orifice plate it is partly reflected and partly transmitted through the orifice. At the same time, for low frequencies, some of the acoustic energy is absorbed as it is converted to vorticity that is created at the orifice edges. In the plane wave frequency range, several quasi-steady models have been proposed for the linear passive acoustic properties of thin ducted orifice plates. Examples of such theories, which have shown good agreement with measurements, are the theory for low Mach numbers described by Åbom *et al.* [2] and the theory by Durrieu *et al.* [3], which also is applicable at higher jet Mach numbers where flow compressibility effects are present. These theories predict a frequency independent scattering, where the reflection increases and the transmission decreases with increasing Mach number.

To improve the understanding of the acoustic properties of constrictions Direct Noise Computations (DNC) are performed using compressible Large Eddy Simulation (LES). With this method the interaction between the flow and incoming waves can be captured, as well as sound generating mechanisms. To compute the scattering, i.e. reflection and transmission of incoming waves, an acoustic two-port model is used. To validate the method the results are compared to the measurements and theory presented Åbom *et al.* [2]. Earlier linear 2D simulations have been performed by Kierkegaard *et al.* [4] for the same configuration, but at a lower Mach number, showing good agreement with the measurements.

*Address all correspondence to this author.

Using LES to simulate linear acoustic propagation and scattering is a relatively new research area. Previous it has been done by Föller *et al.* [5,6], who successfully used LES with second order accurate numerical methods to compute the scattering by an area expansion and a t-junction, respectively. They simulated the entire 2-port in one simulation by using completely non-reflecting boundary conditions and different broadband excitation signals at all boundaries. The outgoing waves are then correlated to the different excitation signals and the two port was obtained with a Wiener-Hopf inversion technique.

COMPUTATIONAL METHODS

The equations governing the flow, including the acoustics, are the compressible equations for conservation of mass, momentum and energy, also called the compressible Navier-Stokes equations, together with an equation of state. A derivation of the conservation equations on different forms can be found in e.g. [7]. In conservation form the equations can be written as

$$\frac{\partial \rho}{\partial t} + \frac{\partial (\rho v_i)}{\partial x_i} = 0 \tag{1}$$

$$\frac{\partial (\rho v_i)}{\partial t} + \frac{\partial (\rho v_i v_j)}{\partial x_j} = -\frac{\partial p}{\partial x_i} + \frac{\partial \sigma_{ij}}{\partial x_j} + f_i \tag{2}$$

$$\begin{aligned} &\frac{\partial}{\partial t}[\rho(e+\tfrac{1}{2}v^2)] + \frac{\partial}{\partial x_i}[\rho v_i(e+\tfrac{1}{2}v^2)] = \\ &\qquad -\frac{\partial (p v_i)}{\partial x_i} + \frac{\partial (\sigma_{ij} v_j)}{\partial x_i} - \frac{\partial q_i}{\partial x_i} + f_i v_i \end{aligned} \tag{3}$$

where ρ is the density, v_i is the velocity component in i-direction, e is the internal energy per unit mass, p is the static pressure, σ_{ij} is the viscous stress tensor, f_i is a possible external force field (per unit volume) acting on the fluid (e.g. gravity) and q_i is the heat flux.

In order to close the conservation equations an equation of state is needed. Assuming that air is an ideal gas, we use:

$$p = \rho R T \tag{4}$$

where R is the specific gas constant and T is the temperature.

Air is also assumed to be a Newtonian fluid, which means that the stress due to fluid motion can be assumed to be a linear function of the strain rate, i.e. the gradients of the flow state variables. The viscous stress tensor represents the stress due to fluid motion and is then given by

$$\sigma_{ij} = 2\mu(S_{ij} - \tfrac{1}{3}S_{kk}\delta_{ij}) \tag{5}$$

where μ is the dynamic viscosity, which is a function of temperature, and S_{ij} is the rate of strain tensor, which is defined as

$$S_{ij} = \frac{1}{2}\left(\frac{\partial v_i}{\partial x_j} + \frac{\partial v_j}{\partial x_i}\right) \tag{6}$$

The heat flux is assumed to obey with Fourier's law:

$$q_i = -K\frac{\partial T}{\partial x_i} \tag{7}$$

where T is the temperature and K is the heat conductivity, which is a function of the temperature.

Large Eddy Simulation

The turbulent fluctuations that are present in higher Reynolds number flows are included in the equations governing the flow (Eqn. (1 - 3)). So if these equations are solved exactly, with so called direct numerical simulation (DNS), the turbulent fluctuations will be captured. To do this all scales of the turbulent flow have to be resolved and the computational effort increases as O(Re^3). This means that as the Reynolds number is increased DNS becomes computationally very expensive and eventually impossible with the computer resources available today. The turbulence has therefore to be modeled. The most commonly used turbulence models are Reynolds average Navier Stokes (RANS) models. In these models the flow variables are split into a mean and a fluctuating part and equations are solved for the mean variables. If the mean is computed as an ensemble average the mean flow may still be time dependent. However, the range of time-scales in such a case is much smaller than in fully turbulent flows. Furthermore, RANS models are very dissipative, which can cause problems with low amplitude acoustic fluctuations. When the geometry is more complex and RANS cannot capture the dynamics of the flow, Large Eddy Simulation (LES) is the main alternative. This model is computationally still much cheaper than DNS (O(Re^2) instead of O(Re^3)), even though it is much more expensive than RANS.

The idea of LES is that the large energy containing scales, which are coupled to the geometry, are resolved in the simulation, while the small dissipative scales are modeled. The turbulent kinetic energy spectra is then cut somewhere in the middle into a resolved and an unresolved (modeled) part. This is achieved by filtering the Navier-Stokes Equations (Eqn. (1 - 3)) with a spatial low-pass filter. Several types of explicit filters exist, but it is more common to let the discretization scheme itself act as a low-pass filter. As the Navier-Stokes equations are filtered additional terms are introduced in the equations. In order to solve the filtered equations these so called SGS terms have to be modeled. Since the small (unresolved) scales tend to be universal at high Reynolds numbers it is easier to suggest appropriate SGS models then RANS models.

An SGS model should account for the effects of the unresolved scales on the resolved ones and for the most important physical properties of the unresolved scales. The main effect at these scales is dissipation of kinetic energy at these scales, which is one of the effects that one has to model. Instantaneously there is also energy transfer from the smaller to the larger scales, a phenomenon known as backscatter. This effect may be neglected if the spatial resolution is fine enough (i.e. resolving a portion of the inertial subrange). Under such conditions the separation of scales between the energy bearing eddies and the unresolved scales is large enough to ensure small errors.

An alternative to using an explicit modeling of the sub-grid scales is to use implicit LES. With this approach the numerical dissipation present from the discretization is assumed to take care of the dissipation at small scales and thereby accounting for the most important role of the SGS terms. The idea of implicit LES can be described by studying the modified incompressible momentum equation that is satisfied by the numerical filtered solution, which contains numerical errors (e.g. truncation errors):

$$\frac{\partial \bar{v}_i}{\partial t} + \bar{v}_j \frac{\partial \bar{v}_i}{\partial x_j} = -\frac{1}{\rho}\frac{\partial \bar{p}}{\partial x_i} + \nu \frac{\partial^2 \bar{v}_j}{\partial x_i \partial x_j} - \frac{\partial}{\partial x_i}(\tau_{ij}^{SGS} + \tau_{ij}^{num}) \quad (8)$$

where over-lined variables are filtered and τ_{ij}^{num} is additional numerical stresses, which represent the numerical error and is of the order $(\Delta x)^p$ for a p:th order accurate scheme. From Eqn. (8) it can easily be seen that the dissipation from the SGS stresses and the numerical discretization are additive. This implies that by using an appropriate numerical method the numerical scheme can act as an SGS model and no explicit model is needed. The problem is that the numerical dissipation is difficult to control, i.e. the amount of dissipation is not a function of the flow. Therefore it is often argued that it is more physical to use an explicit model together with a low dissipation numerical scheme. At the same time it can be argued that if numerical dissipation already is present in the LES solver, which is the case in all general CFD codes where lower order accurate schemes often are used, it is not desirable to add any additional dissipation in the form of an explicit SGS model. However, if implicit LES is used it is important to be aware of the fact that the result is strongly dependent on the grid resolution and the numerical scheme if the spatial resolution is not adequate (i.e. not well within the inertial sub-range). As the grid is refined and the resolved range is extended towards the Kolmogorov scale, which can be attained nowadays for relatively low Re, LES tends to DNS and thereby the implicit SGS (as well as most explicit SGS) models are in fact *approximations* rather than models in a strict meaning.

The numerical computations presented in this paper have been performed with implicit LES. The reason for this is that the numerical dissipation is large enough and does not require any further enhancement. We also make sure that the spatial resolution is such that a proportion of the inertial sub-range is resolved, see Fig. 5.

Numerical Methods

The simulations have been performed with the general compressible CFD code Edge, which is a node based finite volume code [8].

For the temporal discretization a low storage, four stage, second order accurate Runge-Kutta scheme has been used. This can be considered low accuracy for acoustic problems, but to ensure stability one have to fulfill the Courant Friedrichs Lewy (CFL) condition, which states that the Courant number must be less than one

$$\mathrm{CFL} = \frac{U\Delta t}{\Delta x} \leq 1 \quad (9)$$

where Δt is the time step, Δx is the cell size and $U = |u| + c$ is the maximum physical propagation speed, where u is the convection velocity and c is the speed of sound. The interpretation of this condition is that no physical information is allowed to propagate further than one grid cell at one time step. In the present simulations the maximum Courant number was around 0.6, due to code stabilization problems at higher values, ensuring a very small time-step compared to the spatial discretization size. This implies that the spatial discretization is the most important parameter for the total accuracy of the problem.

The spatial discretization uses a formally second order central scheme. Central schemes have the advantage of having very low numerical dissipation, but the disadvantage that they can introduce unphysical dispersion (i.e. a frequency dependent sound speed) and spurious oscillations, which must be damped numerically to ensure stability. This is achieved by adding a Jameson type of artificial dissipation, to the inviscid terms [9]. Furthermore, by adding the artificial dissipation the numerical dissipation becomes large enough to perform implicit LES.

DETERMINING THE ACOUSTIC TWO-PORT

An acoustic two-port gives the linear relation between the acoustic properties up- and downstream of a duct component as a function of frequency in the plane wave range. There are several different formulations of the two-port and here it is convenient to use the scattering matrix formulation [10]. The scattering matrix (**S**) relates the amplitudes ($\hat{p}_+$ and $\hat{p}_-$) of the incoming and outgoing waves (p_+ and p_-), up- (a) and downstream (b) of the

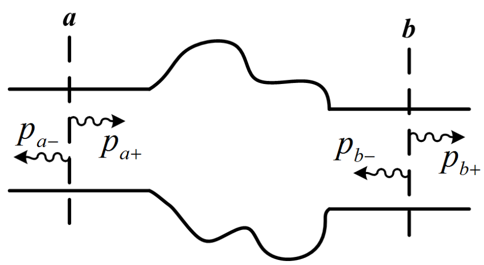

FIGURE 1. DEFINITION OF WAVE PROPAGATION DIRECTIONS FOR WAVES IMPINGING ON AN OBJECT. THE WAVES ARE REFERRED TO A CERTAIN REFERENCE CROSS-SECTION.

component, as shown in Fig. 1. In the general case the scattering matrix can be written as:

$$\begin{pmatrix} \hat{p}_{a-} \\ \hat{p}_{b+} \end{pmatrix} = \mathbf{S} \begin{pmatrix} \hat{p}_{a+} \\ \hat{p}_{b-} \end{pmatrix} + \begin{pmatrix} \hat{p}_a^s \\ \hat{p}_b^s \end{pmatrix}, \qquad \mathbf{S} = \begin{pmatrix} S_{11} & S_{12} \\ S_{21} & S_{22} \end{pmatrix} \tag{10}$$

Where S_{11} is the upstream reflection coefficient, S_{22} is the downstream reflection coefficient, S_{21} is the up- to downstream transmission coefficient, S_{12} is the down- to upstream transmission coefficient and $\hat{p}_a^s$ and $\hat{p}_b^s$ is the amplitude of the generated sound radiated in the up- and downstream directions, respectively. The elements of the scattering matrix will be complex and contain information about both the amplitude of the coefficients and a possible phase shift taking place between the up- and downstream sampling positions used for the acoustic variables.

To determine the four unknown scattering-matrix elements it is assumed that the level of the incoming sound is high enough to neglect the generated sound. Furthermore, two independent cases, with different incoming waves, are required. In this work this is achieved by performing two simulations with the acoustic excitation up- and downstream of the component, respectively. Using the result from these two cases the scattering-matrix can be calculated from:

$$\begin{pmatrix} S_{11} & S_{12} \\ S_{21} & S_{22} \end{pmatrix} = \begin{pmatrix} \hat{p}_{a-}^1 & \hat{p}_{a-}^2 \\ \hat{p}_{b+}^1 & \hat{p}_{b+}^2 \end{pmatrix} \begin{pmatrix} \hat{p}_{a+}^1 & \hat{p}_{a+}^2 \\ \hat{p}_{b-}^1 & \hat{p}_{b-}^2 \end{pmatrix}^{-1} \tag{11}$$

Where 1 denotes the first case and 2 the second case.

When sampling of acoustic variables is performed it usually has to be done at a distance from the studied object. The reason is that it is desirable to avoid sampling in acoustic near fields or in regions with high flow fluctuation levels. In acoustic near fields there can be higher order modes, which rapidly decays further away from the object, and this might influence the result. In regions of high flow fluctuation levels it is difficult to extract the low amplitude acoustic fluctuations. When the sampling is performed at a distance from the object, the phase of the scattering matrix elements contain not only a possible phase shift due to the object, but also the phase shift from the wave propagation between the object and the sampling positions. To avoid this, the scattering matrix can be moved to the object with Eqn. (12) [11].

$$\mathbf{S}' = \mathbf{T}_+ \mathbf{S} \mathbf{T}_-^{-1} \tag{12}$$

Where $\mathbf{S}'$ is the modified scattering matrix that has been moved to the component, and has a phase that corresponds to the phase shift added by the object, and $\mathbf{T}_\pm$ are:

$$\mathbf{T}_+ = \begin{pmatrix} e^{ik_{a+}x_a'} & 0 \\ 0 & e^{ik_{b+}x_b'} \end{pmatrix}, \qquad \mathbf{T}_- = \begin{pmatrix} e^{-ik_{a-}x_a'} & 0 \\ 0 & e^{-ik_{b-}x_b'} \end{pmatrix} \tag{13}$$

Where x_a and x_b are the distances from the up- and downstream measuring positions to the object and k_+ and k_- are the wave numbers for waves propagating in the up- respectively downstream directions at the up- (a) and downstream (b) sides of the object. The phase of the modified scattering matrix is sensitive to the flow Mach number, meaning that a small error in the latter can give a significant effect on the scattering matrix, as shown by Holmberg [12].

Plane Wave Decomposition

To compute the scattering matrix the sampled acoustic pressure (p') and velocity (u') fluctuations have to be decomposed into the up- and downstream propagating waves p_+ and p_-, respectively. To compute these waves the following plane wave decomposition method is used:

$$p_+ = \frac{1}{2}[p' + \rho_0 c_0 u'], \qquad p_- = \frac{1}{2}[p' - \rho_0 c_0 u'] \tag{14}$$

The method is based on the assumptions that the acoustic fluctuations can be written as a sum of up- and downstream propagating waves, Eqn. (15), and that the plane wave relation, Eqn. (16), is valid. These assumptions are valid in a free field where there is no dissipation, but the presence of walls where the velocity is forced to zero can cause deviations from the theory.

$$p' = p_+ + p_-, \qquad u' = u_+ - u_- \tag{15}$$

$$p_\pm = \pm \rho_0 c u_\pm \tag{16}$$

Flow Noise Suppression

In turbulent flows the acoustic waves are accompanied by turbulent fluctuations. In order to get accurate results this so called flow noise has to be suppressed. The properties that separates the acoustic fluctuations from the non-acoustic flow fluctuations is that they have a harmonic time dependence and they propagate with the speed of sound plus / minus the mean flow velocity in the up- and downstream directions, respectively. Furthermore, at each cross section along the pipe, they can be projected on specific mode shapes depending on frequency. For low frequencies only the plane wave mode, where the acoustic variables are constant at a cross-section, can propagate through the duct. In the case of externally excited incoming waves, these also have to be separated from the flow generated sound. To extract these waves the following methods have been used:

1. The amplitude of the externally excited waves is set significantly higher than the amplitude of the generated noise, in order to be able to neglect the latter. At the same time non-linear effects have to be avoided so the amplitude cannot be set too high. It has therefore been investigated how the result is affected by the excitation amplitude.

2. In the plane wave frequency range, which is considered here, the acoustic pressure and velocity are constant over cross-sections of the duct. Turbulent fluctuations are therefore reduced by using the cross-section average fluctuations:

$$p' = \frac{1}{A}\int_A p\, dA, \qquad u' = \frac{1}{A}\int_A u\, dA \tag{17}$$

3. To suppress non-acoustic fluctuations the characteristics based filtering (CBF) method proposed by Kopitz *et al.* [13] has been used. By using the known acoustic propagation speed ($c \pm u$), the acoustic fluctuations are averaged over n successive cross-sections, according to:

$$p_+(x,t) = \frac{1}{n}\sum_{i=1}^{n} p_+(x+\Delta x_i, t+\Delta x_i/(c+u)_i) \tag{18}$$

$$p_-(x,t) = \frac{1}{n}\sum_{i=1}^{n} p_-(x+\Delta x_i, t-\Delta x_i/(c-u)_i) \tag{19}$$

   where Δx is the distance between the planes. In the results presented here averaging has been performed with 10 and 19 cross-sections up- and downstream of the constriction, respectively.

4. The time signals are phase averaged and then Fourier transformed. This is in order to suppress fluctuations at frequencies other than the excitation frequencies and to extract the amplitude and phase of the latter.

FIGURE 2. THE CONSTRICTION SEEN FROM THE SIDE. THE DASHED LINES INDICATE THAT THE DUCTS ARE LONGER THAN SHOWN IN THE FIGURE.

Theoretical Model

The results presented in this paper are compared to the incompressible quasi-steady theory presented in [2]. The scattering matrix is then determined by:

$$\mathbf{S} = \frac{1}{2+MC_L}\begin{pmatrix} MC_L & 2 \\ 2 & MC_L \end{pmatrix} \tag{20}$$

Where M is the inlet Mach number and $C_L = \Delta p/(\frac{1}{2}\rho U^2)$ is the pressure loss coefficient. The latter is analytically determined as $C_L = (\frac{1}{\sigma\Gamma} - 1)^2$, where σ is the area contraction ratio of the orifice and Γ is the vena contracta, which is determined from incompressible theory, giving a pressure loss coefficient of 22.2 for the studied configuration. The vena contracta is the ratio of the effective flow area through the orifice and the orifice area, which is smaller than one due to flow separation at the upstream edge of the orifice.

MODEL SETUP

The geometry of the constriction studied is shown in Fig. 2. The area contraction ratio of the constriction is 0.28, the duct diameter is 5.7 cm and the plate thickness is 2 mm. The up- and downstream ducts are 15.2 respectively 35 duct diameter long.

The geometry is meshed with a structured hexahedral mesh, using an o-grid. The mesh has 4.9 million nodes. The grid looks the same at each cross-section of the duct, with finer cells at the radius of the plate edges. In the axial direction the cell size at the plate is one tenth of the plate thickness. The cells are then stretched towards in- and outlet, with a stretching factor of 2.2 %, to a maximum cell length of 6.5 mm.

Boundary Conditions

The walls in the domain are specified as slip and adiabatic, i.e. the wall normal velocity is forced to zero and there is no heat transfer to or from the walls. Physically, slip walls imply neglecting the boundary layer at the wall. To validate that the assumption of slip walls does not influence the scattering, simulations have been performed also with no-slip wall boundary conditions at either just the plate or at both the plate and the duct wall. The result are not presented here, but they showed that the choice of wall boundary condition does not significantly influence the scattering [14]. The reason for using slip boundary conditions is that it gives significantly lower dissipation of propagating waves and it preserves the validity of Eqn. (16) by keeping the theoretical mode shapes, which are destroyed close to the wall with the no-slip boundary condition as the acoustic velocity is forced to zero. The slip boundary condition also decreases the mesh size, since a coarser mesh can be used next to the duct wall.

At the inlet boundary the normal velocity and density are specified to give an inlet Mach number of 0.08 and the tangential velocity components are set to zero. At the outlet boundary a constant static pressure of 10^5 Pa has been specified.

Exciting Acoustic Waves

To excite acoustic waves up- or downstream of the constriction time varying in- or outlet boundary conditions are used, where an oscillating part is added to the mean value. At the inlet the velocity and density oscillations are in phase and the amplitudes are related with the plane wave relation $u' = (c/\rho_0)\rho'$.

Due to the reflective outlet boundary condition it is not desirable to use a broadband excitation signal [15]. At the same time the computational cost is too high to use a step sine method, i.e. one simulation per studied frequency. The excitation signal therefore consists of a sum of sine waves, with a random phase shift and frequencies that are harmonics of the same base frequency.

Analytical Waves

An evaluation of how the noise in the scattering matrix results is affected by lowering the excitation amplitude has been performed by adding fluctuations corresponding to an analytical wave to the flow fluctuations computed with a LES. The analytical wave is created as a sum of sine waves for first the case of an upstream and then a downstream excitation. For each sine wave the up- and downstream wave components are calculated at each evaluation cross-section, using a defined excitation amplitude and scattering matrix, the sound and flow speeds from the simulation, the cross-section positions and assuming non-reflecting in- and outlet boundaries. At each plane the sum of the fluctuations corresponding to each sound wave is calculated and used to determine the acoustic pressure and velocity fluctuations using the inverse of Eqn. (14). Finally, these acoustic fluctuations are added to the flow fluctuations and the evaluation of the scattering matrix is performed.

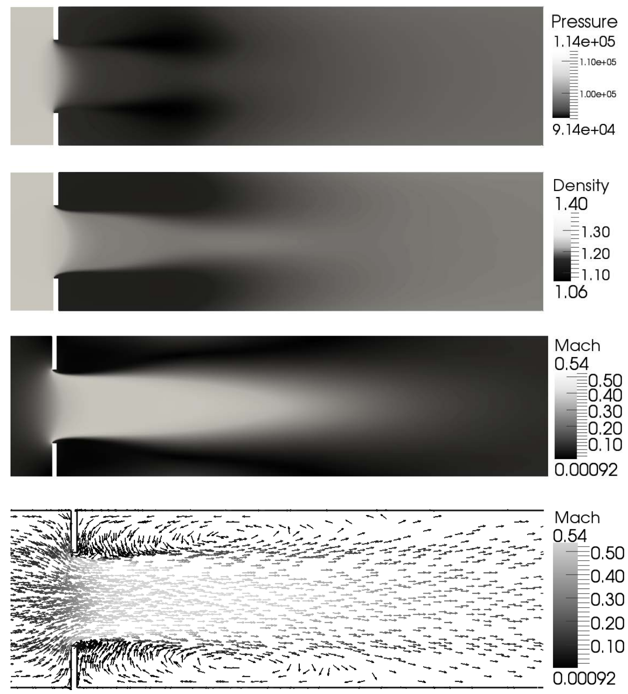

FIGURE 3. ZOOM IN ON THE FLOW THROUGH THE ORIFICE PLATE. THE TOP THREE FIGURES SHOW THE MEAN FIELD AND THE BOTTOM FIGURE SHOWS THE NORMALIZED IN-PLANE MEAN VELOCITY VECTORS COLOURED BY MACH NUMBER.

RESULTS

The flow is computed with an inlet Mach number of 0.08, giving a Reynolds number of around 120000. The mean flow is shown in Fig. 3. It can be observed that a jet is formed as the air is forced through the small opening and a large pressure drop occurs, with some pressure recovery further downstream. The density field further shows significant compressibility effects, as is also reflected in the high Mach number of the jet. The vena contracta of the jet is clearly visible, as the flow separation at the upstream edge of the plate reduces the effective flow area.

Figure 4 shows a snapshot of the instantaneous flow field. Here it can be observed that the flow is highly unsteady, with vortex shedding at the plate edges. Figure 5, of the centreline axial velocity spectra downstream of the plate, shows that at around one duct diameter (5.7 cm) downstream of the plate the spectra resemble a Kolmogorov spectrum, with a -5/3 slope of the velocity fluctuations. This indicates that part of the inertial sub-range in the turbulent kinetic energy spectrum is resolved. Further upstream the spectra has a different character due to the fluctuations in the jet core and breakdown not being those of homogeneous, isentropic turbulence that the -5/3 slope represents.

FIGURE 4. ZOOM IN ON THE INSTANTANEOUS FLOW THROUGH THE ORIFICE PLATE. THE TOP FIGURE SHOWS THE MACH NUMBER AND THE BOTTOM FIGURE SHOWS VORTEX CORES.

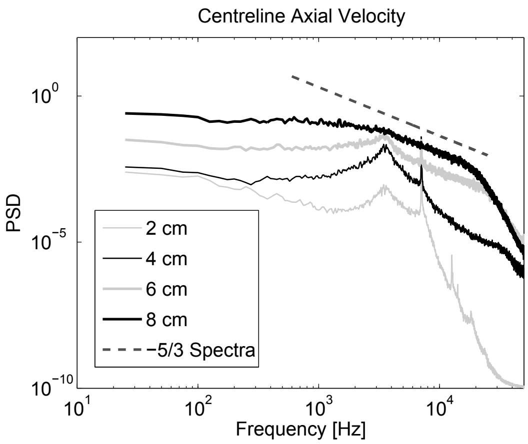

FIGURE 5. POWER SPECTRAL DENSITY OF THE AXIAL VELOCITY FLUCTUATIONS IN FIVE POINTS AT THE CENTRELINE DOWNSTREAM OF THE PLATE.

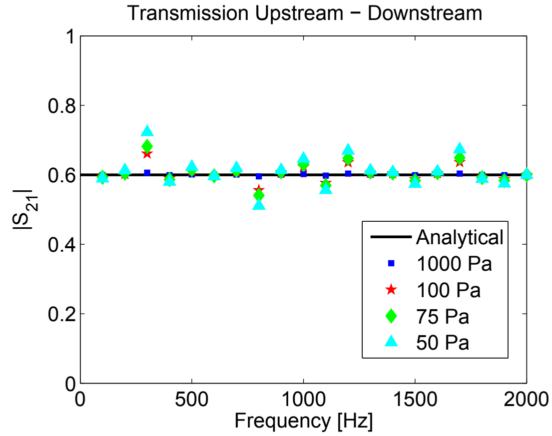

FIGURE 6. AMPLITUDE DEPENDENCE OF THE UP- TO DOWNSTREAM TRANSMISSION COMPUTED WITH THE ANALYTICAL WAVES. THE AMPLITUDES ARE GIVEN PER FREQUENCY COMPONENT.

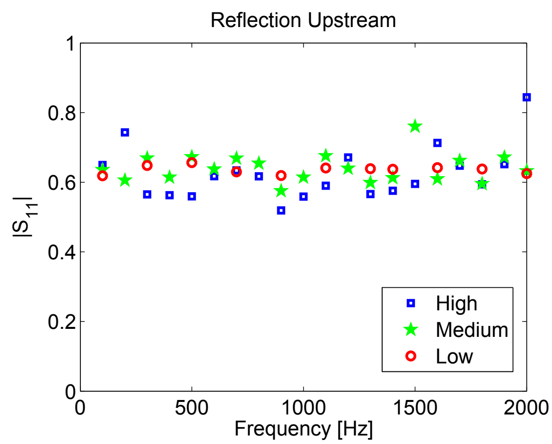

FIGURE 7. AMPLITUDE DEPENDENCE OF THE UPSTREAM REFLECTION.

Excitation Amplitude

As mentioned above the excitation amplitude cannot be set arbitrarily high, since it will lead to non-linear effects, at the same time as it has to be high enough to drown the flow noise.

The theoretical lower limit for the excitation amplitude has been tested with the analytical waves described above. As expected the random error in the computed scattering increases when the amplitude is decreased. The largest influence on the result is observed for the amplitude of the up- to downstream transmission, which is shown in Fig. 6.

To check for non-linear effects the scattering matrix was simulated with three different total excitation amplitudes. Figure 7 shows the result for the amplitude of the upstream reflection, which by the analytical waves was shown to be insensitive to lowering the amplitude. It can be observed that the result depends on the excitation amplitude, indicating the presence of non-linear effects. The noise introduced as the amplitude is increased is due to energy being transferred between different harmonics and all excited frequencies are harmonics of the lowest frequency. As the amplitude is reduced the non-linear effects are reduced and since the present non-linearities do not seem to significantly influence the average level of the elements, it is assumed that the lowest excitation level can be considered linear.

A measure for non-linear effects can be expressed in terms of the amplitude of the velocity fluctuations relative to the mean velocity in the orifice. Without externally excited waves the velocity fluctuations are below 1.5 % of the mean velocity. For the simulations presented above the maximum velocity fluctuations are around 12 %, 6 % and 3 % of the mean velocity, respectively. These results indicate that non-linear effects start to appear when the amplitude of the acoustic velocity fluctuations becomes higher than around 1 % of the mean velocity. This can be compared with the low Mach number measurements performed by Testud *et al.* [1], for which non-linear effects did not appear until the acoustic fluctuations increase to around 10 % of the mean velocity.

Comparison With Measurements

The computed scattering has been compared to measurements and theory presented in Åbom *et al.* [2]. The amplitude and the phase of the scattering matrix are shown in Fig. 8 and Fig. 9, respectively. The simulations show reasonable agreement with the measurements for the amplitude of the scattering matrix elements and for the phase of some of the elements.

The discrepancy observed for the phase in Fig. 9 is likely due to errors when moving the measured scattering matrix elements from the measuring position to the object. This procedure has been shown to be sensitive to the Mach number [12], which is easier to retrieve from a simulation than from a measurement, and an error could result in the observed frequency dependence. For example, a 20 % error in the Mach number at either side of the object could result in a phaser error of the order of 1.4 for the transmission coefficients and this could be the case due to the velocity being measured only at one point.

The amplitudes of the scattering matrix elements for the downstream coefficients (downstream reflection and down- to upstream transmission) in Fig. 8 are in good agreement with the measurements. The upstream coefficients (upstream reflection and up- to downstream transmission) are however slightly higher in the simulations. Studying the theory it is observed to agree well with the measured upstream coefficients, while it proposes slightly higher values for the downstream coefficients. This discrepancy could be due to compressibility effects that are neglected in the theory, but clearly are present in the flow due to the high jet Mach number.

According to the theory the reflection and transmission coefficients are the same from both directions and depend on the parameter MC_L. The Mach number is clearly the same in both the simulations and the theory, but the pressure loss coefficient turned out to be somewhat different; 26.7 in the simulations compared to the theoretical value of 22.2. This does however affect the theoretical scattering matrix less than the discrepancy observed in Fig. 8. Furthermore, the trend from changing this parameter, which was also observed in the measurements, indicate that reducing it will reduce the upstream reflection, but it will at the same time increase the up- to downstream transmission, which is not desirable.

Another fact that is important to consider is that Kierkegaard *et al.* [4] have performed linear 2D simulations of the scattering by the same geometry (using the mean flow from another simulation) with very good results compared to the measurements at a lower Mach number ($M = 0.054$). The difference in the scattering matrix could then come from differences in the mean flow, but they should be smaller than the differences due to slip or no-slip walls that have been shown not to be of importance [14]. The fact that the linear 2D simulations by Kierkegaard *et al.* [4] gave good results then indicates that the discrepancy has to do with the interaction between the wave and the orifice plate.

The fact that both the reflection and the transmission of waves coming from the upstream direction become too high indicates that less of the acoustic energy is converted to vorticity in the simulations and/or that there is less dissipation. The dissipation in the duct should however be small at least for the lowest frequencies. Furthermore, the conversion of acoustic energy is better captured for waves coming from the downstream direction. This dependency on propagation direction could be explained by the acoustic wave seeing the geometry differently from the two directions due to the flow field. A wave coming from the upstream side clearly impinges on the upstream edge of the orifice, while the jet, with the vena contracta effect, partly hides the downstream edge from downstream excited waves. Errors in the prediction of the interaction between the wave and the sharp edge could therefore give a larger effect for waves coming from the upstream direction. An insufficient grid resolution at the plate could give such effect, but a grid refinement of this area did not significantly change the result.

CONCLUSIONS

The linear low frequency scattering of plane waves by a constriction has been studied through LES. The effect of the excitation amplitude has been investigated, showing that there is a fine line between keeping it low enough to avoid non-linear effects, but at the same time high enough to avoid errors from flow noise. The performed simulations indicate that non-linear effects start to appear when the amplitude of the acoustic velocity fluctuations becomes higher than around 1 % of the mean velocity in the orifice.

The simulated scattering matrix has been compared to measurements and theory for an inlet Mach number of 0.08. The result for the downstream reflection and the down- to upstream transmission show good agreement with the measurements. At the same time the amplitude of the upstream reflection and partly also the up- to downstream transmission become slightly too large compared to the measurements and the theory. However, it should be noted that the trend of a frequency independent scattering is present in both the simulations and the measurements. Since both the reflection and the transmission of waves coming from the upstream direction are too high, it is likely that not enough of the acoustic energy is converted to vorticity at the plate

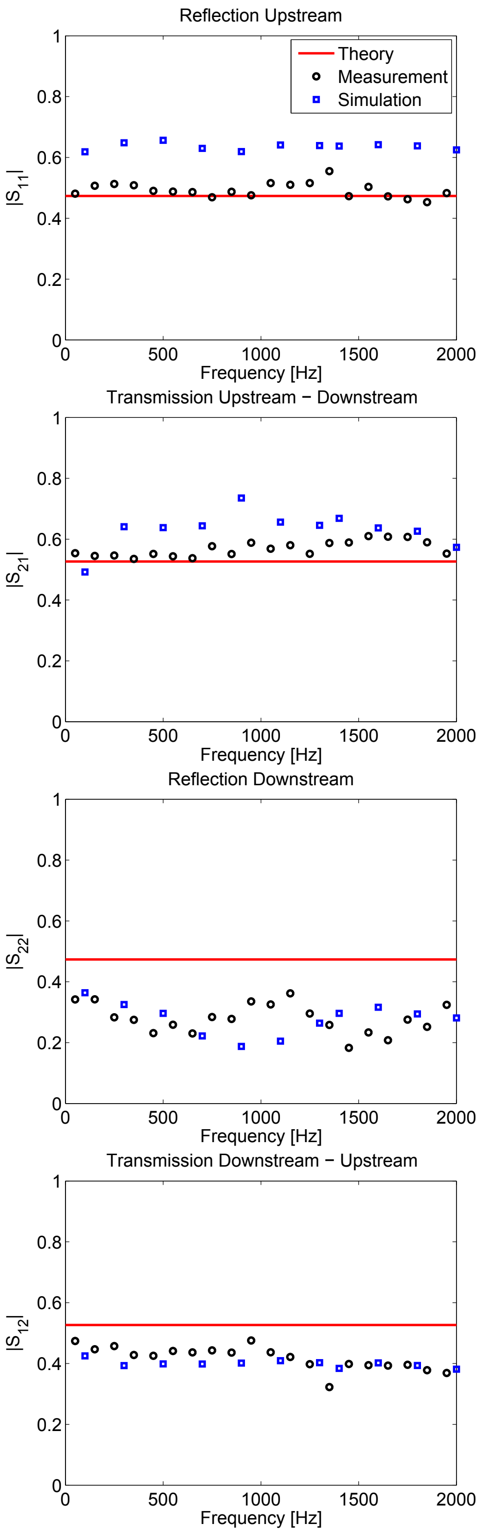

FIGURE 8. THE AMPLITUDE OF THE SCATTERING MATRIX COMPARED TO MEASUREMENTS AND THEORY.

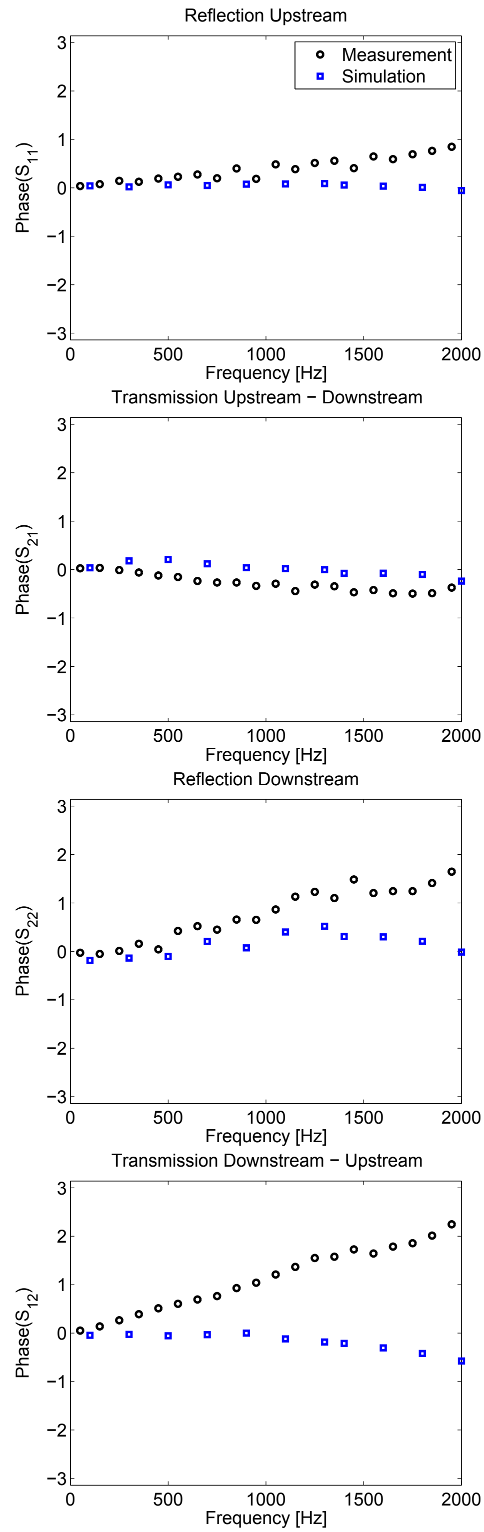

FIGURE 9. THE PHASE OF THE SCATTERING MATRIX COMPARED TO MEASUREMENTS.

edges in the simulations. The fact that the linear 2D simulations performed by Kierkegaard *et al.* [4], at a lower Mach number ($M = 0.054$), gave good results as compared to the measurements further indicates that the discrepancy is related to the interaction between the wave and the orifice plate.

ACKNOWLEDGMENT

The KTH CICERO center is acknowledged for the financial support. High Performance Computing Center North (HPC2N) and The National Supercomputer Centre in Sweden (NSC) are acknowledged for supplying the necessary computational resources.

REFERENCES

[1] Testud, P., Aurégan, Y., Moussou, P., and Hirschberg, A., 2009. "The whistling potentiality of an orifice in a confined flow using an energetic criterion". *Journal of Sound and Vibration,* ***325***(4-5), pp. 769–780.

[2] Åbom, M., Allam, S., and Boij, S., 2006. "Aero-Acoustics of Flow Duct Singularities at Low Mach Numbers". In 12th AIAA/CEAS Aeroacoustics conference, Cambridge, Massachusetts, USA. AIAA paper 2006-1287.

[3] Durrieu, P., Hofmans, G., Ajello, G., Boot, R., Aurégan, Y., Hirschberg, A., and Peters, M., 2001. "Quasisteady aero-acoustic response of orifices". *The Journal of the Acoustical Society of America,* ***110***, p. 1859.

[4] Kierkegaard, A. ., Efraimsson, G., and Boij, S., 2008. "Acoustic propagation in a flow duct with an orifice plate". In ISMA conference, Leuven, Belgium.

[5] Föller, S., and Polifke, W., 2010. "Determination of acoustic transfer matrices via large eddy simulation and system identification". In 16th AIAA/CEAS Aeroacoustics Conference, Stockholm, Sweden. AIAA paper 2010-3998.

[6] Föller, S., Polifke, W., and Tonon, D., 2010. "Aeroacoustic characterization of t- junctions based on large eddy simulation and system identification". In 16th AIAA/CEAS Aeroacoustics Conference, Stockholm, Sweden. AIAA paper 2010-3985.

[7] Anderson, J., 1995. *Computational fluid dynamics: the basics with applications*. McGraw-Hill. ISBN 0-07-113210-4.

[8] Eliasson, P., 2001. EDGE, a Navier-Stokes Solver for Unstructured Grids. Scientific report FOI-R–0298–SE, FOI-Swedish Defence Research Agency. ISSN 1650-1942.

[9] Jameson, A., Schmidt, W., and Turkel, E., 1981. "Numerical solutions of the Euler equations by finite volume methods using Runge-Kutta time-stepping schemes". *AIAA paper,* ***81-1259***.

[10] Glav, R., and Åbom, M., 1997. "A general formalism for analyzing acoustic 2-port networks". *Journal of Sound and Vibration,* ***202***(5), pp. 739–747.

[11] Lavrentjev, J., Åbom, M., and Boden, H., 1995. "A measurement method for determining the source data of acoustic two-port sources". *Journal of Sound and Vibration,* ***183***(3), pp. 517–531.

[12] Holmberg, A., 2010. "Experimental determination of aeroacoustic sources in low mach number internal flows". Licentiate thesis, KTH. TRITA-AVE 2010:69, ISSN 1651-7660.

[13] Kopitz, J., Bröcker, E., and Polifke, W., 2005. "Characteristics-based filter for identification of planar acoustic waves in numerical simulation of turbulent compressible flow". In 12th Int. Congress on Sound and Vibration (ICSV), Lisbon, Portugal.

[14] Alenius, E., 2010. "CFD of Duct Acoustics for Turbocharger Applications". Licentiate thesis, KTH. ISBN 978-91-7415-828-1.

[15] Gentemann, A., Yuen, S., and Polifke, W., 2004. "Influence of boundary reflection coefficient on the system identifiability of acoustic two-ports". In 11th Int. Congress on Sound and Vibration (ICSV), St. Petersburg, Russia.